.FINAL REPORT: .

SOLAR CELL PERFORMANCE

MATHEMATICAL MODEL

Prepared for the

California Institute of Technology

Jet Propulsion Laboratory

Under Contract JPL 952548

By

M. J. Barrett, M. B. Hornstein, and R. H. Stroud

Exotech Incorporated
525 School Street, S.W.
Washington, D.C.   20024

June 15, 1970

TRSR 70-12

FINAL REPORT:

SOLAR CELL PERFORMANCE

MATHEMATICAL MODEL

Prepared for the

California Institute of Technology

Jet Propulsion Laboratory

Under Contract JPL 952548

_by

M. J. Barrett, M. B. Hornstein, and R. H. Stroud

-Exotech·Incorporated
.525 School Street, S.W.
.Washington, D.C.   20024

June 15, 1970

ABSTRACT

A computer program has been prepared to calculate the electrical characteristics of silicon solar cells as a function of cell parameters and space environmental factors. The program, in Fortran IV, computes short-circuit current and the current and power at selected voltages to permit construction of a current-voltage curve characteristic of the solar cell. Environmental factors considered are illumination intensity and spectrum, cell temperature, and exposure to corpuscular radiation.

TABLE OF CONTENTS

INTRODUCTION

This is the final report of a program to generate a useful mathematical model for silicon solar cell performance in space. The model, begun under previous contract*, has been extended, adjusted to a closer fit of available measurements, and incorporated in software for computer simulations of specific designs and environments for solar cell performance.

Previous quarterly reports have presented details of the work. In this final report, the analytical effort is summarized. Beginning with a review of the solar cell and its applications, the presentation is arranged to describe first the characteristics of the cell (Section I), then details of optical considerations (Section II), and then radiation exposure effects (Section III). These are the main parts to the model and computer code. The code itself (delivered separately to JPL) is described in Section IV. Recommendations for further development are presented in Section V.

I. MODEL OF THE SILICON SOLAR CELL

A. Solar Cell Parameters

Modern solar cells for spacecraft applications are typified by Figure 1. The cell area may be from 1 x 2 cm to 3 x 3 cm, with a cell thickness of 8-14 mils (dimensions are conventionally given in these heterogenous units). A junction is formed about 0.5 micron $(5 \times 10^{-5}$ cm) below the sunward surface; this junction separates the thin "surface" region of n-type silicon from the thicker "base" region of p-type silicon. For the sunward side, the electrical contact is in the form of a bar along one edge and a number of thin grid lines extending from it across the surface. The dark side contact generally completely masks the back surface of the cell.
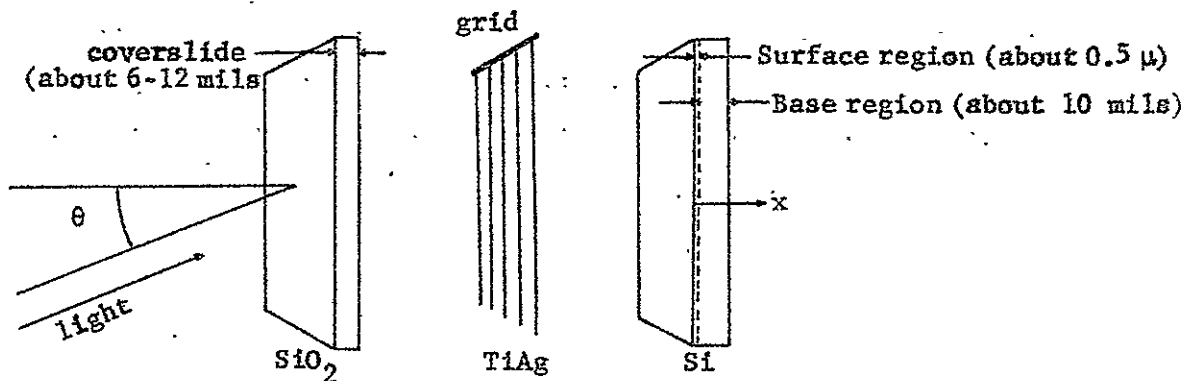
Figure 1. Exploded view of typical solar cell.

Illumination of this device results in the sunward surface being a fraction of a volt positive with respect to the back surface. A current is thereby induced in an electrical connection between the front bar and the back contact. This is not equal, however, to the current generated by the sun (photovoltaic current), for some of the photovoltaic current is returned through the solar cell itself, in accordance with its diode property. The division

2.

of current leads to the solar cell equation, which states that the electrical current flowing from a solar cell equals the difference between the photovoltaic current I_L produced in it, and the diode current I_D lost in it.

The output of a solar cell depends on a large number of independent factors. First, the intensity of sunlight and the angle of incidence are important. A cell directly facing the sun receives the maximum possible sunlight. If it deviates from this direction by an angle θ, as shown in Figure 1, the radiant energy striking the cell is reduced by the cosine of θ. As the angle increases, edge effects, especially when a coverslide is used, make the reduction deviate slightly from this law. Measurement must be relied on for each specific geometry when extreme accuracy is required for solar cells illuminated at large angles from the perpendicular.

The output of solar cells has frequently been characterized by the short-circuit current I_{sc}, the open circuit voltage V_{oc}, and the power and voltage of the cell near its maximum power point. While these parameters do characterize the electrical output, in theoretical work more fundamental terms are to be preferred. These are the photovoltaic current I_L, the diode parameters I_o and V_o, and the internal series resistance R. These four parameters are chosen since it is a more straight-forward exercise to determine from semiconductor physics how they are affected by the environment and history of a solar cell. .

Observing that a solar cell acts as a diode operating in opposition to a current source, Prince and Wolf proposed the solar cell equation (ref. 1). Our only change to this equation is to replace the usual expression AkT/q by the single parameter V_o. We propose calling V_o the "characteristic voltage" of the solar cell, and write the equation for the current I as

$$I = I_L - I_o \left[e^{(V+IR)/V_o} - 1 \right] \tag{1}$$

where V is the voltage across the cell.

Does the theoretically - inspired Eq. 1 indeed reproduce an actual solar cell output? We have developed curve - fitting techniques that select values of the parameters very well. Two samples are presented in Figure 2 with the fitted solar cell equations. These comparisons demonstrate the accuracy often possible with the solar cell equation. They also demonstrate magnitudes of the parameters. (Voltages here are given in millivolts and currents in milliamperes. The resistance of typical cells is generally lower, about 0.1 ohm, than in these examples.) Deviations of measurements from the solar cell equation have been reported. Wolf and Rauschenbach (ref. 3) have recommended that the current source be assumed to be shunted by two diodes with different characteristic voltages. The revised solar cell equation, in our notation, would then take the form

$$ I = I_L - I_{o1} \left[e^{(V+IR_{s1})/V_{o1}} - 1 \right] - I_{o2} \left[e^{(V+IR_{s2})/V_{o2}} - 1 \right] \qquad (2) $$

This has the immediate advantage of allowing two extra parameters for curve fitting, and the disadvantage of relating these parameters to the individual solar cell and its environment. The rationale for the extra diode term must be developed if it is to be adopted in a general mathematical model. Recognizing that a solar cell can have voltage and material gradients along its junction surface can lead to such composite diode terms. Further, Ladany (ref. 4) has derived a silicon diode expression to replace the pure exponential in Eq. 1 by a sum of exponentials. These studies, valuable in extending our insight into the action of the solar cell, have not yet led to reliable formulas for engineering use. Although a higher accuracy in matching a given I-V curve can be achieved, the simpler solar cell equation with its four parameters is to be preferred for parametric studies.

The space environment operates on the solar cell parameters in ways that are imperfectly understood. Of course, the uncertainties

4.
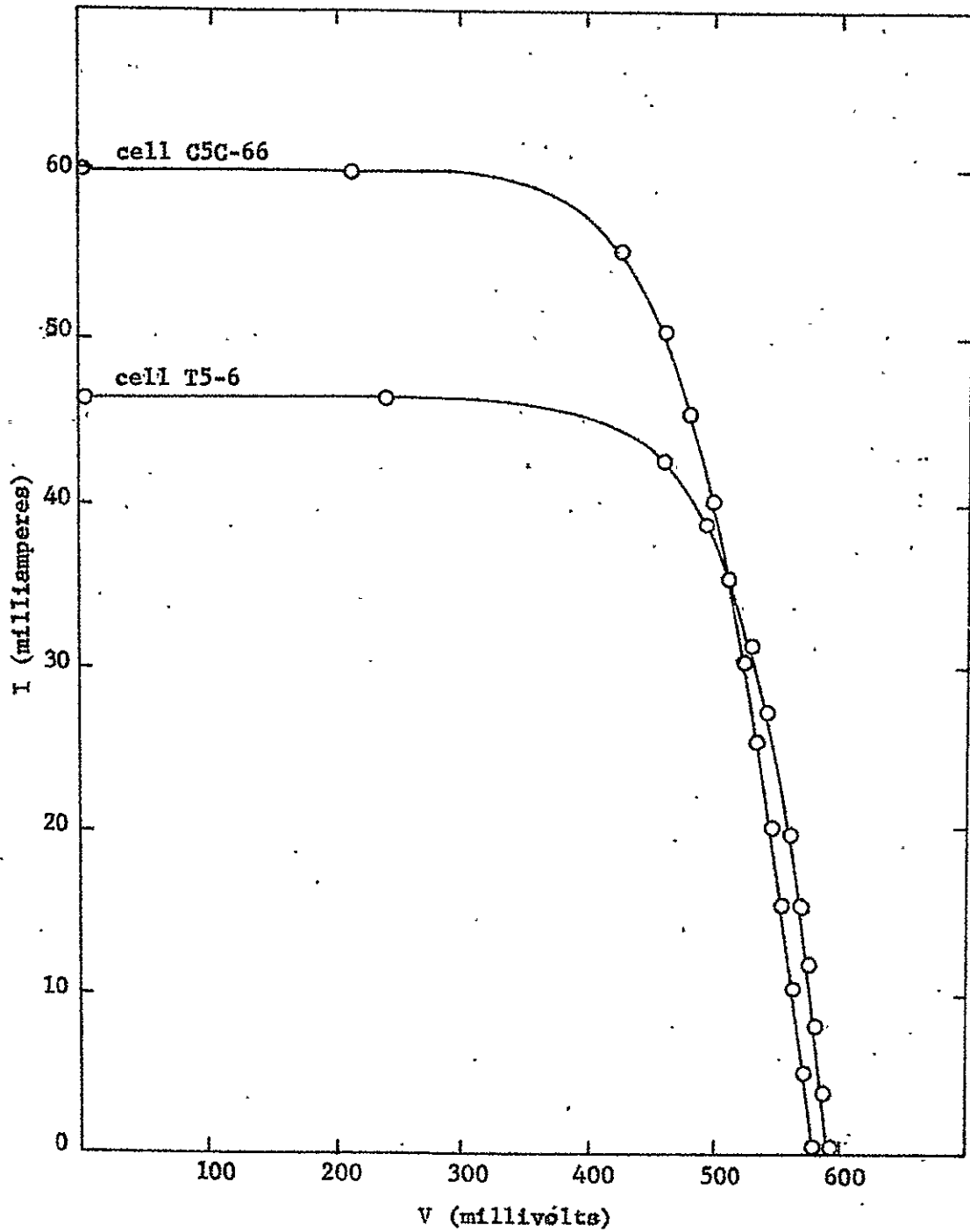
Figure 2. Comparison of measured I-V curves (Ref. 2) with
points computed with the solar cell equations:

$$I = 60.2 - 1.675 \times 10^{-4} (e^{(V + .791I)/45.34} - 1) \quad \text{cell C5C-66}$$

$$I = 46.3 - 1.625 \times 10^{-4} (e^{(V + .322I)/46.98} - 1) \quad \text{cell T5-6}$$

in radiation fluences in space add to the difficulty. As a result, theory and experimental data from the laboratory are often the best that is available to predict changes in solar cell output in space. By correlating theory with laboratory data, the relation of these four parameters to environment and exposure can be obtained.

B. Photovoltaic Current Density

To determine the magnitude of the photovoltaic current produced by the solar cell, it is necessary to follow the sequence of events from light absorption, through carrier diffusion and drift, to recombination at the junction. Damage due to corpuscular radiation and the dependence of the physical parameters on temperature and illumination are to be taken into account in this sequence.

The equations obeyed are the continuity equation for the minority carrier current[*]

$$\frac{1}{q}\frac{dj}{dx} - \frac{n(x)}{\tau(x)} + G(x) = 0 \qquad (3)$$

the current equation

$$J = qD\frac{dn}{dx} + q\mu E n \qquad (4)$$

the damage equation

$$\frac{1}{L^2} = \frac{1}{L_o^2} + K\Phi \qquad (5)$$

---

[*]the symbols used throughout are given in the glossary.

6.

the diffusion relation

$$L^2 = \tau D \qquad (6)$$

and the Einstein relation

$$q D = \mu k T \qquad (7)$$

These equations, applicable to the minority carriers in the base region, have their counterparts for the surface region, using a separate set of values for the material parameters. The photovoltaic current I_L is, of course, the sum of the current densities J into the junction from both sides, multiplied by the area of the solar cell that is exposed to the light source. This is somewhat less than the actual front surface area, due to masking of up to 10% of the surface by the front contact.

The effect of temperature on the diffusion coefficient D of minority carriers in silicon may be determined from measured values of the temperature - mobility relationship. The measurements (ref. 5) show that for electrons the mobility varies as $T^{-2.5}$, and that for holes it varies as $T^{-2.7}$. Therefore, D_n varies as $T^{-1.5}$ and D_p varies as $T^{-1.7}$.

The effect of temperature of the minority carrier lifetime τ is composed of many factors, most of which depend upon the specific processing that the cell has been subjected to. Each of the process steps changes the number, type, and energy level of the recombination centers that determine the lifetime. The temperature dependence of many types of recombination centers has not been described in the literature. It was therefore necessary to assume a relationship that is consistent with experimental results. If τ is taken as proportional to $T^{5.5}$, the temperature coefficient of I_L in the region about $300^{\circ}K$ is $0.05\%/^{\circ}C$, which is consistent with the photovoltaic current measurements given by Reynard (ref. 6) and others. This back - calculation of temperature - dependence of τ from observed temperature - dependence of I_L is an empiricism worthy of further review.

1. Base Region Contribution

The current equation is simplified in the base region since the electric field E is negligible in a uniformly doped region. Combining the current equation and the continuity equation then yields

$$D_n \frac{d^2 n}{dx^2} - \frac{n}{\tau} + G(x) = 0 \tag{8}$$

We assume for boundary conditions that the minority carrier density n vanishes at the junction and at the cell surface. Equation 8 is then solved by computer iteration using a variable interval for the distance x in a difference approximation to the differential.

A variable increment technique is used to increase the accuracy of the difference approximation and to minimize computer time. The difference equation approaches the differential equation as the interval size approaches zero. Therefore small increments, particularly near the junction where the current equation (Eq. 4) is used, are desirable. However, use of very small increments throughout the solar cell thickness requires a large number of increments and, consequently, more computer time. For this reason a compromise was made: small intervals in the critical region near the junction and increasingly larger ones in the less significant areas deeper into the cell. The technique necessarily requires a more complex form of the difference equation than normally used.

8.
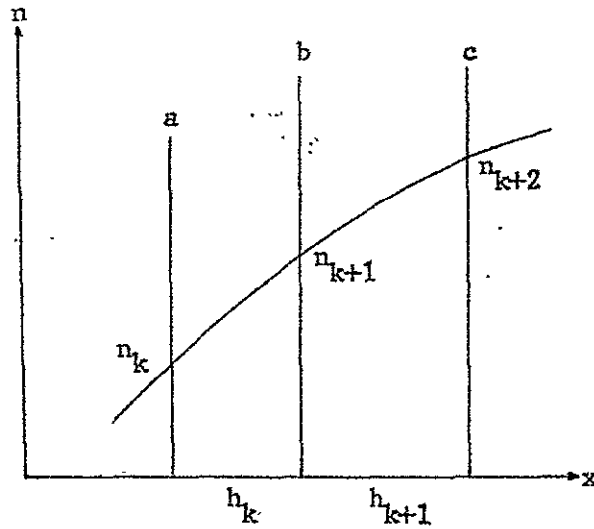
Figure 3. Construction of variable mesh h_k to approximate the curve $n(x)$ at points n_k

The difference approximation, for a variable width interval, can be derived with the aid of Figure 3. The slopes of the curve between a and b, and between b and c are approximated as constants. The first derivative of the curve, evaluated at b, is taken as the average of the slope on either side of b, i.e.

$$\frac{\Delta n}{\Delta x}\Big|_b = \frac{1}{2}\left(\frac{n_{k+2}-n_{k+1}}{h_{k+1}} + \frac{n_{k+1}-n_k}{h_k}\right) = \frac{n_{k+2}h_k + n_{k+1}\left(h_{k+1}-h_k\right)-n_k h_{k+1}}{2h_k h_{k+1}} \tag{9}$$

The second derivative at b is determined from the slopes on either side of b. It is then

$$\frac{\Delta^2 n}{\Delta x^2}\Big|_b = \frac{n_{k+2}h_k - n_{k+1}\left(h_k + h_{k+1}\right) + n_k h_{k+1}}{h_k h_{k+1}\left(h_k + h_{k+1}\right)} \tag{10}$$

Using equation 9 and 10 in the continuity equation, with the field terms eliminated, the minority carrier concentration can be

found from

$$n_{k+2} \frac{2}{h_{k+1}\left(h_k + h_{k+1}\right)} = n_{k+1}\left(\frac{2}{h_k h_{k+1}} + \frac{1}{L_{k+1}^2}\right) - n_k \frac{2}{h_k\left(h_k + h_{k+1}\right)}$$

$$- \frac{G_{k+1}}{D_n} \tag{11}$$

To solve Eq. 11, it is necessary to have values for n_o and n_1 . We assume the boundary conditions that the carrier density vanishes at the junction and at the cell surface. This assumption was also made by Bullis and Runyan (ref. 7) but other boundary conditions have been assumed. We guess n_1 and calculate all the higher values of n_k. We repeat this guessing of n_1 until we arrive at a satisfactory value for the carrier density at the cell surface.

The accuracy of the initial n_1 and the iteration technique are of importance in determining how often the calculation must be repeated before obtaining zero carrier density at the contact sur-face of the cell. If the guess for n_1 is too small, then the values of n_k determined via Eq. 11 will change sign in the cell. If it is too large, the n_k at the back of the cell will fail to be zero. Iterating on n_1 leads to as close an estimate as is desired. One possible technique for convergence is to compare each n_k with n_{k-1} and if there is a sign change then stop, increase the estimate for n_1 by a nominal 10% and repeat. When there is no sign change, de-crease the estimate for n_1 by a nominal 5% and repeat until a sign change occurs. Then increase by 1% until there is no sign change. Such a convergence routine can obviously be carried to any level of accuracy in the estimate of n_1 for the solar cell in question, by taking advantage of this sign change. Our present technique is described on page 31.

10.

The current equation put into this difference form relates n_1, the minority carrier concentration at the distance h_1 from the junction, to the current from the base into the junction.

$$.J = q D_n n_1 / h_1 \qquad (12)$$

since the boundary conditions require that n vanish at the junction.

2. Surface Region Contribution

The surface region of a solar cell, typically only 0.2 to 0.5 microns thick, contributes a minor amount to the photovoltaic current. Calculation of this contribution with the technique used for the base region is complicated by several factors. To begin with, the normal process of junction formation by in-diffusion of n-type impurity atoms results in a complementary error function type of distribution of donor atoms. The concentration N(x) is related to the concentration N(0) at the surface by the temperature-dependent atomic diffusion coefficient D and the process time t by

$$N(x) = N(0) \; \text{erfc} \left(x/\sqrt{4Dt} \right) \qquad (13)$$

In solar cell manufacture, a typical value of N(0) appears to be 10^{20} atoms/cm^3. The product Dt, if unknown from the process, can be calculated if the junction depth is known. At the junction, N(x) must equal the impurity concentration of the base material.

The code uses a polynomial approximation to the complementary error function.

$$\text{erfc} \left(y \right) = \left(c_4 n^4 + c_3 n^3 + c_2 n^2 + c_1 n \right) \frac{2}{\sqrt{\pi}} e^{-y^2} \qquad (14)$$

where
$$n = \frac{1}{1 + 0.381965\,y}$$

$$c_1 = 0.12771538$$

$$c_2 = 0.54107939$$

$$c_3 = 0.53859539$$

$$c_4 = 0.75602755$$

$$y = x/\sqrt{4\,\mathcal{D}t}$$

The non-uniform impurity concentration over the surface region also causes variation in the minority carrier diffusion coefficient D_p. The term D_p is the diffusion coefficient for holes and should not be confused with $\mathcal{D}$, the atomic diffusion coefficient used above. Since D_p does not change uniformly with concentration, the variation with impurity concentration shown by Conwell (ref. 8) is used. Since no simple equation will fit the entire curve, it was decided that the best approach was a series of empirical equations. These are:

for $\quad N < 10^{15}$ $\qquad D_p = 13.0$ $\qquad$ (a)

$\quad 10^{15} < N < 10^{16}$ $\qquad D_p = 52.0 - 2.6 \log N$ $\qquad$ (b)

$\quad 10^{16} < N < 10^{17}$ $\qquad D_p = 56.16 - 2.86 \log N$ $\qquad$ (c) $\qquad$ (15)

$\quad 10^{17} < N < 10^{18}$ $\qquad D_p = 82.86 - 4.42 \log N$ $\qquad$ (d)

$\quad 10^{18} < N < 10^{19}$ $\qquad D_p = 41.28 - 2.1 \log N$ $\qquad$ (e)

$\quad N < 10^{19}$ $\qquad D_p = 1.0$ $\qquad$ (f)

For the surface region, where the field is not negligible, the continuity equation becomes

$$G(x) - \frac{p}{\tau_p} + p\,\mu_p\,\frac{dE}{dx} - \mu_p\,E\,\frac{dp}{dx} + D_p\,\frac{d^2 p}{dx^2} = 0 \qquad (16)$$

12.

where   P = concentration of minority carriers (holes)

τ_p = lifetime of holes

μ_p = mobility of holes

E = field due to impurity gradient = $\dfrac{kT}{q}\dfrac{1}{N}\dfrac{dN}{dx}$

Using equations 13, 14, 15 and 16 we solve the continuity equation on the computer by putting it in the form of a difference equation, in the manner demonstrated in the previous section.

The inclusion of these equations in the final program would unnecessarily lengthen the computing time. The routines for the surface region, therefore, were run separately, with varying temperature, junction depth, radiation and illumination intensity. The variation of the surface contribution to the minority current density J with these factors was curve fitted as

$$J = (0.01408 + 0.005956\, \ell n\, x_j - 0.01411e^{-5.353\, L})$$
$$(T + 400)\, (U \cos \theta / 140)\ mA/cm^2 \tag{17}$$

The minority carrier diffusion length L (in microns) is taken at the first increment in the base region. The assumption here is that L, computed in the base region near the junction for base region calculations, is a measure of the amount of radiation exposure the surface region has received. For the thickness of practical solar cell surface regions, the damage is uniform and this value of L is an indicator of the exposure.

Use of this expression to estimate the surface region contribution to the photovoltaic current permits us to bypass a more involved calculation such as used for the major contribution by the base region.

C. · Diode Characteristics

The characteristic voltage V_o of the diode response by the solar cell appears to be independent of temperature, radiation exposure, and illumination. For this reason, the expression AkT/q normally found in the solar cell equation has been replaced by a constant V_o in our solar cell equation (Eq. 1). This implies that A is inversely proportional to temperature, and measurements by Kennerud (ref. 9) replotted in Figure 4, back this up. The lack of any clear dependence of V_o on radiation exposure was demonstrated earlier (ref. 10). Analysis of solar cell response curves under different illumination intensities has also failed to show any clear changes in V_o.
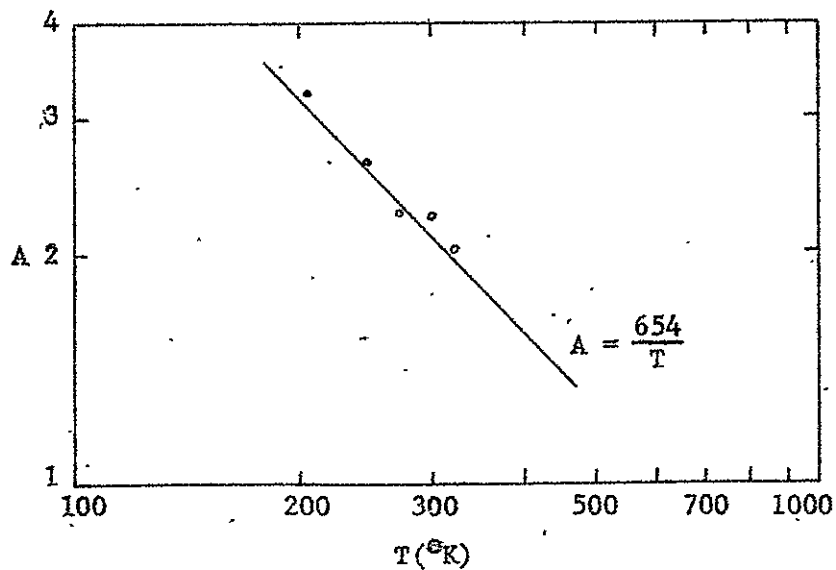
Figure 4. Reported values of A, versus temp-
erature T, for typical n/p silicon
solar cells. After reference 9.

The antithetic situation occurs with respect to the diode saturation current I_o. A functional relationship to light intensity, temperature, and radiation exposure has been developed in this study from a combination of theory and indirect measurements.

Relating the diode saturation current to illumination can be accomplished from experimental data on the open circuit voltage V_{oc}, remembering that the photovoltaic current is proportional to illumination. According to Ritchie and Sandstrom (ref. 11) V_{oc} increases at a rate of 0.2 mV/mW/cm^2 with increasing illumination intensity U. I_o can be calculated from this using the standard solar cell equation. If I_o is plotted against ℓn U, as in Figure 5, the curve can be approximated by a straight line. We therefore make I_o proportional to ℓn U in the mathematical model.

Figure 5. Variation of diode current with illumination intensity.

A similar technique was employed to establish the temperature variation of I_o. Theoretically I_o is proportional to exp $(-E_g/2kT)$. Assuming the photovolta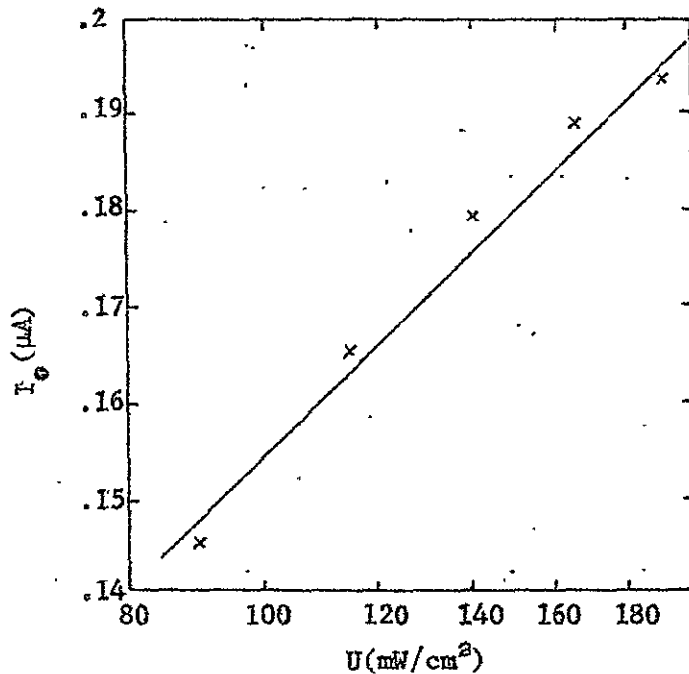ic current density increases 0.05%/°C, and the series resistance is negligible, the theoretical relationship yields a temperature coefficient of V_{oc} as 0.56%/°C. This value falls within the range of Reynard's early experiments (ref. 6) indicating the correctness of the theoretical expression.

Shockley's analysis (ref. 12) for diode junctions provides a theoretical expression for I_o that is inversely proportional to the base region minority carrier diffusion length near the junction. This establishes a radiation dependence of I_o through the damage equation (Eq. 5). Thus, we expect the diode current of a solar cell to increase with increasing radiation damage. This trend has been observed (ref 13) in an analysis of ATS-1 spacecraft solar cells. Coupling this with the temperature and illumination intensity relationship yields, in mA/cm²

$$I_o = (L_o/L)[1.57 \, \ell n \, (U \cos \theta) - 3.36] \exp (-6492/T) \times 10^5 \qquad (18)$$

The factor cos θ relates the solar illumination intensity U to the intensity observed on the solar cell surface as a function of the aspect angle θ. This expression assumes the cell is illuminated on its front surface. I_o here is a current density and is to be scaled appropriately to the particular solar cell area under consideration.

D. Cell Resistance

The series resistance of a solar cell is a composite of resistance terms due to current flow across the bulk region, along the surface region to the contacts, and from silicon to front and back contacts (ref. 14). Each of these terms logically would behave differently under radiation exposure. As a consequence, careful analysis of resistance effects would require one first to partition

R among its components, and then scale these components as they change with radiation exposure. Some uncertainty is obvious in this scheme (even if the effect of radiation on silicon resistivity were known), since manufacturing tolerances would vary the components from cell to cell. Finally, discontinuous events such as the lifting of a contact would be difficult to predict. This would lead to a value of R much greater than normally expected.

Cell resistance generally plays a small part in the behavior of a solar cell. In this study it is considered a constant due to lack of information on its variation with radiation exposure. Experimental measurements would be useful in establishing the quantitative nature of the increase in R. Whether the nature of the dopant affects the change, whether it is linear with exposure, whether temperature plays a significant role, and whether the nature of the damage depends on the bombarding particles, are questions to be answered by such measurements.

II. CARRIER GENERATION

The light generated rate of production of minority carriers
G(x), occurring in the continuity equation (Eq. 3), is a function
dependent on the illumination intensity, spectrum, and absorption
coefficient of light in silicon. The non-analytic variation of
spectrum and absorption coefficients with wavelength of light pre-
cludes an analytic solution. Therefore, the contributions to G(x)
from different parts of the light spectrum must be considered in-
dividually. This is accomplished through numerical integration of
the relationship

$$G(x, \lambda) = \alpha(\lambda)H(\lambda)\left(\frac{\lambda \cos \theta}{2 \pi \hbar c}\right) e^{-\alpha(\lambda) x/\cos \theta'} \tag{19}$$

over all values of wavelength λ to which the solar cell responds.
This region is normally taken as 0.4 to 1.1 microns. The small
fraction of incident light reflected at the solar cell surface,
normally on the order of two or three percent, has been neglected
in this expression.

Values of the absorption coefficient $\alpha(\lambda)$ and the spectral
irradiance $H(\lambda)$ are given in Table 1 for an illumination intensity
of 140 mW/cm^2, AMO (air mass zero) conditions, and a temperature
of 300°K. Variation of the illumination intensity causes a pro-
portional variation in $H(\lambda)$ for all λ. Variation in the air mass
condition, e.g., reduction of the spectrum to AM1 conditions by
atmospheric absorption, varies the spectrum since the absorption is
selective and changes with atmospheric conditions. In this case the
individual values of $H(\lambda)$ must be changed appropriately. Temper-
ature will effect the absorption coefficient. Macfarlane and
Roberts (ref. 17) give the absorption coefficient as

$$\alpha \doteq A\left[\frac{1}{1-e^{-B/T}}\left(\frac{\hbar\omega - E_g - kB}{\hbar\omega}\right)^2 + \frac{1}{e^{B/T}-1}\left(\frac{\hbar\omega - E_g + kB}{\hbar\omega}\right)^2\right] \tag{20}$$

18.

Table I

Absorption Coefficient of Silicon and Sunlight Intensity
as a Function of Wavelength

λ in microns, $\alpha(\lambda)$ in cm^{-1} (Ref. 15)

$H(\lambda)$ in watts/cm^2 - μ (Ref. 16)

λ	$\alpha(\lambda)$	$H(\lambda)$
0.40	7.50×10^4	0.1540
0.45	2.58×10^4	0.2200
0.50	1.18×10^4	0.1980
0.55	7.00×10^3	0.1950
0.60	4.65×10^3	0.1810
0.65	3.33×10^3	0.1620
0.70	2.42×10^3	0.1440
0.75	1.69×10^3	0.1270
0.80	1.12×10^3	0.1127
0.85	7.95×10^2	0.1003
0.90	3.80×10^2	0.0895
0.95	1.80×10^2	0.0803
1.00	7.30×10^1	0.0725
1.05	2.08×10^1	0.0665
1.10	4.40×10^0	0.0606

where: A is a constant

B $= 600^{\circ}$K (for silicon)

$\hbar\omega$ = energy of incident light (in eV)

E_g = energy gap of the semiconductor (1.1 eV. in silicon)

k = Boltzmann's constant

Since E_g varies very slowly with temperature (-0.00013 eV/$^{\circ}$C for silicon) (ref. 18) the quantities $\left[(\hbar\omega - E_g - kB)/\hbar\omega\right]^2$ and $\left[(\hbar\omega - E_g + kB)/\hbar\omega\right]^2$ can be considered constant for each wavelength, making α proportional to $\left[1/(1-e^{-B/T}) + 1/(e^{B/T}-1)\right]$. At $\lambda = 1.1\,\mu$, where $\hbar\omega$ is very close to E_g, the value of α changes only 7% between 250°K and 300°K. Since light in this region of the spectrum contributes only a small number of carriers, the effect may be neglected. At lower wavelengths the variation is even smaller. If the above quantity is designated as f, and (f - 1) is plotted as a function of B/T, as in Figure 6, a straight line results. The equation which fits this line with a maximum deviation of less than 1%, is

$$\ell n\,(f-1) = 1.201 - 1.171\,\frac{B}{T} \qquad 1.6 \leq \frac{B}{T} \leq 2.4 \qquad (21)$$

From equation 21, the relationship between α and T can be shown to be

$$\alpha\,(\lambda,T) = \alpha\,(\lambda,300)\,\frac{3.323e^{-702.6/T}+1}{1.319} \qquad (22)$$
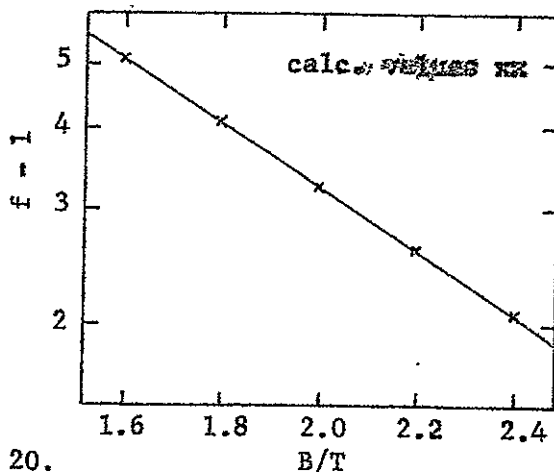
Figure 6. Relationship of absorption coefficient to temperature.

20.

III. RADIATION EFFECTS

A. Proton Shielding

The thickness of a solar cell is comparable to the distance a proton can travel in silicon when its energy is typical of protons found in space. Shielding by a coverslide and self-shielding by the solar cell are consequently important. This is especially significant when one considers the proton energy - dependence of damage.

The distance of travel, or range R, is often related to the incident proton energy E_o by formulas of the form

$$R = R_o E_o^n \tag{23}$$

The equation is not exact, but good fits can be provided over limited ranges of E_o. Table 2 is such a fit to tabulated data.

Table 2

Values of R_o and n for proton range - energy relationships and corresponding energy intervals.[*]

Energy (MeV)	R_o (mg/cm^2)	n
$0.0 \leq E < 0.3$	2.81	0.995
$0.3 \leq E < 0.8$	3.95	1.277
$0.8 \leq E < 2.0$	4.11	1.460
$2.0 \leq E < 200$	3.42	1.726

---

[*] computed from data in ref. 19

The range formula implies that the energy of a proton along its track can be calculated from the residual distance it is to travel before stopping. The relation is not exact, for there is some straggling of the individual tracks of protons of the same energy, but this is generally quite small. The average straggling, as a fraction of R, decreases with proton energy E_o and it is less than 4% for 100 keV protons (ref. 19). Thus, we treat the range equation as being exact and compute a proton energy $\left(E_o^n - \frac{x}{R_o} \right)^{1/n}$ for protons of initial energy E_o which have traveled a distance x in silicon. When monoenergetic protons of an omnidirectional fluence strike the solar cell surface, the effects of slant penetration cause a spectrum at depth x.

A coverslide of thickness t will remove protons of energy E_o and incident angle θ with the normal if their range R is less than the path length $t/\cos\theta$ through the coverslide. It will also reduce the energy of a transmitted proton to E given by

$$E = \left[E_o^{n} - \frac{t}{R \cos\theta} \right]^{1/n} \qquad (24)$$

The differential proton spectrum striking the solar cell due to a monoenergetic, isotropic unit flux penetrating the coverslide can be derived from this expression and is

$$\dot\Phi_p (E) = \frac{nt E^{n-1}}{R_o (E_o^n - E^n)^2} \qquad (25)$$

for energies E less than the energy of a proton penetrating at normal incidence, as calculated from Eq. 24.

The total proton fluence at any depth z in the solar cell assembly is related to the proton fluence in space by

$$\dot\Phi_p (E_o, z) = nz \int_0^{E_t} \frac{\dot\Phi_p (E_o) E^{n-1}}{R_o (E_o^n - E^n)^2} dE \qquad (26)$$

These equations permit calculation of localized proton damage
in solar cells with coverslides, given the appropriate damage
equivalence. This is presented in the next section.

B. Proton Damage

The proton damage coefficient K_p is the measure of decrease in
minority carrier diffusion length due to a fluence Φ of protons (K_p
equals the incremental increase in the quantity $1/L^2$ with incre-
mental increase in Φ). The damage is due to Rutherford scattering
of protons, which dislodges silicon atoms from their lattice position.
Hence, the proton energy dependence of K_p is approximately given by
$1/E$, which is the energy dependence of the Rutherford scattering cross
section. The threshold for dislodging atoms corresponds to a minimum
proton energy of about 0.0001 MeV.

Crowther, et al. (ref. 15) have found a flattening of the energy
dependence of K_p below about 0.5 MeV. This effect may correspond to
an annealing mechanism whereby a dislodged atom has not been pushed
far from its site, and has a high probability of return. The follow-
ing equations fit these measurements for 1 ohm-cm p-silicon and pro-
vide a ratio for higher resistivity p-silicon that agrees with measure-
ments by Denney and Downing (ref. 20).

$$K_p(E) = 1.2\, \Omega^{-0.75}\, E^{-0.9} \times 10^{-5} \qquad \left[E > 3\ \text{MeV} \right] \qquad (27)$$

$$K_p(E) = 1.92\, \Omega^{-0.75}\, e^{-1.04}\, (E/.962)^{-0.85} \times 10^{-5} \qquad \left[3 > E > 1 \right] \qquad (28)$$

$$K_p(E) = 1.92\, \Omega^{-0.75}\, e^{-1.08E} \times 10^{-5} \qquad \left[1 > E > 10^{-4} \right] \qquad (29)$$

Because proton energy changes rapidly with depth of penetration
into the cell, and because the damage coefficient K_p is so dependent
on proton energy, damage by protons of less than about 5 MeV results
in a highly nonuniform minority carrier diffusion length across the cell.

23.

C. Electron Shielding

When a solar cell is covered with t grams/cm^2 of coverglass the electron flux at the cell surface due to isotropically incident monoenergetic electrons of energy E is a spectrum over lesser energies and is dependent on the thickness of the shielding. Here, however, deflections in the individual electron paths complicate the analytic determination of the shielding effect. A weighting factor, derived from a study of Monte Carlo results (ref. 21), enables us to determine the effective damage coefficient $K_e(E,x)$ at depth x into the cell as a fraction of the damage coefficient of the incident electrons $K_e(E)$. The weighting relationship is given by

$$K_e(E,x) = K_e(E) \exp [-10(x+t)/E^{1.6}] \qquad (30)$$

where x + t is the areal density in gm/cm^2 of material penetrated to the site of the damage being considered.

D. Electron Damage

The damage coefficient K_e for electron damage in p-type silicon has been fitted empirically as shown in Figure 7. We neglect to study fits for n-type silicon since electron damage effects are negligible in the surface region, compared to those in the base region. We plotted the square root of measured values of K_e versus electron energy. For crucible - grown p-type silicon of resistivity 10.6 ohm-cm, the measured points, shown in Figure 7, can be connected by two straight line segments. That a straight line results over the energy 1-40 MeV indicates that a recombination center requiring two defects may be involved (ref. 21). Below 1 MeV, sufficient data are not available for such a conclusion, but a straight line curve fit can be presented.

This fitting of the data from ref. 22 and the dependence on electrical resistivity discussed above, give the damage coefficient as

24.

$$K_e(E) = (10/\Omega)^{0.5}(1.2 \ln 2.17E)^2 \times 10^{-10} \cdot \left[E > 1\,\text{MeV} \right] \qquad (31)$$

$$K_e(E) = (10/\Omega)^{0.5}(0.67 \ln 4E)^2 \times 10^{-10} \qquad \left[1 > E > .25 \right] \qquad (32)$$

$$K_e(E) = 0 \qquad \left[.25 > E \right] \qquad (33)$$

where Ω is the resistivity in ohm-centimeters and E is the electron energy in MeV. The expression to fit measurements between 1 and 40 MeV will underestimate the damage for lower energies. Below 1 MeV, the second factor in equation 31 can be replaced by $(0.67 \ln 4E)^2$. This fits the measurement at 0.6 MeV and the generally observed "apparent" threshold of 250 keV.
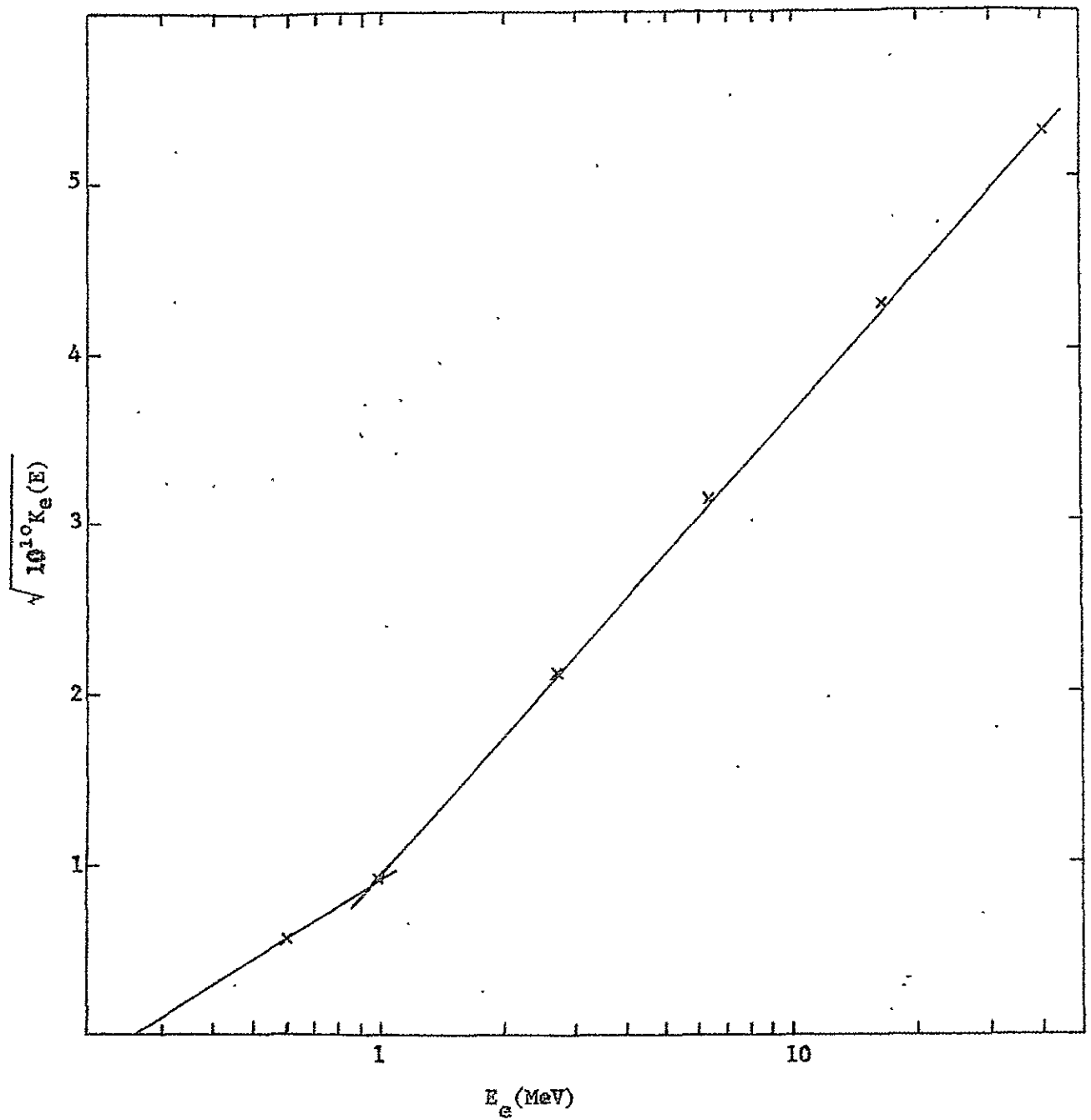
Figure 7. A plot of the square root of the electron damage coefficient
versus electron energy (Data points for p-type silicon,
having a resistivity of 10.6 ohm cm, from ref. 22)

IV. PROGRAM MODULE DESCRIPTIONS

The theory described in the previous sections has been incorporated in a computer program to provide estimates of the simultaneous effects of environmental factors on solar cells. The function of the program is twofold: the determination of the solar cell parameters I_L and I_o; and the associated I-V curve under various environmental conditions, including radiation damage by electron and proton spectra. The program is modular, i.e., a main program accompanied by several subroutines. The main program collects the data necessary to describe the solar cell and its environment, and calls each appropriate subroutine when needed. Each subroutine performs a specific task and is discussed individually below.

The environmental input consists of the temperature, the illumination intensity, and up to ten each of proton and electron energies with their associated fluences. Each fluence is considered to be incident isotropically. By suitable choices of energies and fluences, continuous particle spectra can be approximated. Particle energies are restricted to values below 200 MeV for protons and below 40 MeV for electrons. Particles with energies above these limits are ignored by the program due to lack of data on high energy damage coefficients.

Optical parameters, as given in Table 1, are stored in the program. A list of other necessary input variables and their assumed values is given as Table 3. The values may be changed as desired, but care must be taken to retain the specified dimensions. More detailed discussions follow in the subroutine descriptions.

Table 3. Input Variables

Variable	Definition	Stored Value
XLO	initial base region minority carrier diffusion length at 300°K	150 microns
D	base region minority carrier diffusion coefficient at 300°K	35 cm^2/sec
RHO	base region resistivity	10 ohm-cm
VO	solar cell characteristic voltage	43 mv
R	solar cell series resistance	0.1 ohm
T	solar cell thickness	14 mils
XJU	junction depth	0.5 microns
CT	coverslide thickness	6 mils
TEMP	temperature	300°K
U	illumination intensity	140 mW/cm^2
THETA	incident angle of illumination with respect to normal incidence	0.0°
EOP (I)	proton energies*	0.0 MeV
EHP (I)	proton fluences	0.0 protons/cm^2
EOE (I)	electron energies	0.0 MeV
PHE (I)	electron fluences	0.0 electrons/cm^2
M	number of points considered in the difference equation solution	200
INA	number of beams approximating each isotropic proton fluence	50
A(I)	absorption coefficients of light in silicon	see Table 1
H(I)	spectral irradiance obtained from the Johnson spectrum	see Table 1
CIN	index of refraction of light in silicon	3.8

*(I in this table is a running index.)

28.

A. Subroutine A B S C I S

Subroutine A B S C I S computes the increment thickness HX(K) necessary for the difference equation calculation, and the depth into the cell DX(K) of each corresponding point. The first 20 increments are of equal width delta; the remaining values of HX(K) are given by (K-20) delta. Therefore any error induced by the unequal increment technique occurs away from the junction. Such a compromise between equal and unequal increments reduces the degree of approximation in the critical region near the junction, resulting in a more accurate evaluation of the minority carrier concentration and, consequently, the photovoltaic current density.

The number of points M is set at 200. Testing the program with a greater number of points (smaller increments) shows an insignificant change in the output.

B. Subroutine LIGHT

The rate of production of minority carriers per cm^2 per second due to light absorption is computed for each point provided by subroutine A B S C I S . A Simpson's rule integration over the AM0 Johnson spectrum (ref. 16) from 0.4 to 1.1 microns in 0.05 micron steps is employed. Other spectra, e.g., the tungsten spectrum, may be used by changing the spectral irradiances H(I) in the subroutine's input data to those of the desired spectrum for the wavelengths 0.4, 0.45, ..., 1.1 microns. The method assumes that in any two successive 0.05 micron steps the spectrum approximates a quadratic function. Where this is not the case, e.g., the xenon spectrum, smaller intervals must be employed, or the spectral peaks averaged in the interval.

C. Subroutine COVER

COVER approximates each monoenergetic isotropic proton fluence by a set of 50 beams incident at angles ranging from zero,

with respect to normal incidence, to the maximum angle a proton of
the given energy can have and still penetrate the coverslide and
surface region. This yields a maximum angular increment of 1.8°.
Finer increments can be used but the small change in the output does
not justify the additional computer time. For each angle the proton
energy after penetration and the incremental fluence over the asso-
ciated angular increment are determined. Computation terminates if
the initial proton energy is insufficient to penetrate at normal
incidence, or if the energy after penetration is insufficient to cause
damage.

D. Subroutines PROTON and DAMAGE

Associated with each of the 50 beams determined by COVER is
an angle dependent proton energy profile through the solar cell thick-
ness. PROTON utilizes the range - energy calculations of Janni (ref. 19)
to determine the energy at each point in the cell until such time as: 1)
insufficient energy remains at a point $DX(K)$ to penetrate the next in-
crement $HX(K)$; 2) the energy is below the damage threshold; or 3) the
cell has been completely penetrated. It is assumed that the proton
follows a straight path until one of the above conditions is met. To
each of these energies subroutine DAMAGE associates a damage coef-
ficient. These, in turn, are used with the incremental fluence to de-
termine the degraded minority carrier diffusion length. A damage
diffusion length profile as a function of position in the cell results.
Since the process is repeated for each beam of each initial energy the
final diffusion length profile represents the total damage done by the
approximated proton spectrum.

E. Subroutine ELECT

ELECT is the electron counterpart to subroutines COVER, PROTON,
and DAMAGE. Here, however, the assumption of a non-deflected path can-
not be made. We instead use a weighted damage-coefficient to represent

the damage at a given depth DX(K) in the cell, as described on
page 24. The damage coefficient of the incident monoenergetic
electron fluence is computed first. The effective damage coef-
ficient at depth DX(K) is then determined as a function of the
areal density in gm/cm^2 of material penetrated, i.e., DX(K) plus
the coverslide thickness. The coverslide and silicon densities
are 2.2 and 2.33 gm/cm^2, respectively.

As in subroutine DAMAGE the minority carrier diffusion length
profile is updated using the associated electron fluence and the
weighted damage coefficients. The process is repeated for each
electron energy given as input.

F. Subroutine ROOT

Subroutine ROOT contains the iteration technique to solve
the difference equation approximation of the continuity equation.
The value of the minority carrier concentration at the junction, C(1),
is set equal to zero and an approximation of 10^8 made for its value
at the second point C(2). The approximation of C(2) is then increased
or decreased by an order of magnitude depending on the sign of the
carrier concentration as computed for the back surface of the cell
with the difference equation. A positive sign results when C(2) is
too large and a negative sign when it is too small. The process con-
tinues until the signs differ for two successive approximations, in-
dicating that the correct value of C(2) lies between them. The bi-
section technique is then employed until either the carrier concen-
tration at the back of the cell becomes zero, or two successive values
of C(2) differ by less than 10^{-4} percent.

G. Subroutine TRAP

TRAP contains the actual difference equation approximation of
the continuity equation. It is called by subroutine ROOT and control
is returned if: 1) for a particular C(2), the minority carrier

concentration anywhere in the cell exceeds 10^{30} carriers/cm^3; 2) the minority carrier concentration becomes negative; or 3) the computation for every incremental point is completed.

H. Subroutine CURVE

CURVE utilizes the previously determined data along with the input data to generate the photovoltaic current density I_L, the diode saturation current I_o, points on the resultant I-V curve, and their associated power P. The base region contribution to the photovoltaic current density is determined from the minority carrier concentration gradient at the junction, $C(2)/HX(1)$. The surface region contribution is calculated from the junction depth, illumination intensity, temperature, and degraded minority carrier diffusion length at the junction. Addition of the two current components yields the total photovoltaic current density. Temperature, illumination intensity, and degraded minority carrier diffusion length at the junction are used to approximate the diode saturation current.

A set of the four solar cell parameters is now available. The program is completed with the output of these parameters, environmental data, points on the resultant I-V curve computed from the solar cell equation, and the power associated with each point. An example of the output is given in Table 4.

Table 4. Program Output (Sample)

IL =   40.45 MA   U= 140.0 MW/CM**2
VO =   43.00 MV   TEMP= 300. DEG. K
R   =   0.100 OHM   THETA= 0.00 DEG.
10 =   0.76E-03 MA

I(MA)	V(MV)	P(MW)
0.00	530.9	0.00
4.04	525.9	2.13
8.09	520.5	4.21
12.13	514.3	6.24
16.18	507.3	8.21
20.22	499.1	10.09
24.27	489.1	11.87
28.31	476.3	13.49
32.36	458.4	14.83
36.40	428.2	15.59
36.81	423.7	15.59
37.21	418.6	15.58
37.62	412.8	15.53
38.02	406.1	15.44
38.43	398.2	15.30
38.83	388.6	15.09
39.23	376.2	14.76
39.64	358.7	14.22
40.04	328.9	13.17
40.45	1.1	0.05

The information presented here are the four parameters of the
solar cell equation, given a light intensity U of 140 milliwatts/cm^2,
a sun orientation THETA of 0.00 degrees from the normal, and a
temperature TEMP of 300°K. The parameters are used by the program to
compute voltage V and power P for twenty values of the current I
through the external load.

V. CONCLUSIONS AND RECOMMENDATIONS

A. Conclusions

We now have detailed mathematics available to study solar cell capabilities and design. It transcends previously utilized techniques of viewing the solar cell in terms of equivalences, such as representing non-uniform proton damage as equivalent 1 MeV electron damage, and allows analysis on the level and in the scope of the particular phenomena of interest. For example, the model is capable of predicting the power degradation of solar cells in a combined environment of protons and electrons both of arbitrary energies. Nonuniformity of damage is permitted in the calculations. In the process, it provides the necessary framework to optimize a solar cell coverglass assembly for any particular radiation environment, taking into account the other environmental factors and cell parameters. One measure of the versatility of the model is the list of variables, Table 3, considered by the program.

The computer program encompassing the mathematical model has been used to test the validity of the model relationships. The results are, in general, consistent with experimental evidence as illustrated in previous reports under this contract. Summarizing the results of the testing process we find:

1. V_{oc} decreases with increasing temperature, primarily due to the increase in diode saturation current.

2. P_{max} decreases with increasing temperature, illustrating that thermal effects on this portion of the solar cell I-V curve are dominated by I_o rather than I_L.

3. I_{sc}, V_{oc}, and P_{max} decrease with increasing junction depth beyond 0.2 microns.

4. The surface region is essentially unaffected by irradiation.

In the course of this contract many improvements have been made in the mathematical model generated under JPL contract 952246.

34.

Noteworthy among these are:

1. A technique of unequal increments has been employed in
    the difference equation calculations, which reduces the
    degree of approximation in the critical region near the
    junction. This results in a more accurate evaluation of
    the minority carrier concentration and, consequently, the
    photovoltaic current density.

2. The parameters associated with the surface layer have been
    included, reducing the degree of approximation formerly
    introduced by assuming a constant surface region contri-
    bution to the total photovoltaic current.

3. The analysis of the electron shielding by a coverslide
    has been greatly simplified, facilitating its incorporation
    into the computer program without appreciably extending
    computation time.

4. The study of the diode reverse saturation current has
    lead to a more detailed expression that takes account of
    the response of this parameter to changes in temperature,
    illumination, and radiation exposure.

B. Recommendations

1. Further refinement of the model produced in this work is
recommended. Experimental efforts tailored to an investigation of
specific parameters are needed. When one parameter is being
changed, the others should be measured so that their values can
be placed in the computer calculation. (The lack of complete
measurements makes it difficult to assess many published experi-
mental data.) An experimental program would not only validate
the model, but would point out areas where future analytical effort
is warranted.

2. With respect to low energy protons we have found that
the theoretical expression overestimates the actual damage to the

35.

photovoltaic current in the cases we have analyzed. As discussed on p. 23, the energy dependence of the damage coefficient diminishes at low energies (below 1 MeV). A reasonable extension of this behavior would be for the damage coefficient to decrease as one goes to very low energies. This could explain the low damage rate measured by Statler and Curtin (ref. 23) for 0.27-MeV protons. Laboratory measurement of low energy proton damage, coupled with their analysis via the computer program, is recommended.

3. Extensions of the model to cover present developments appear feasible and should be undertaken. For example, a concentration gradient of lithium in lithium-doped solar cells (ref. 24) and the redegradation process appear to result in a non-uniform residual damage, which subroutine ROOT is uniquely able to handle for these cells. In a separate extension, drift field solar cell performance in an AMO spectrum could be studied.

4. The model should be applied to the evaluation of solar cell designs for specific flight missions, to relate design parameters to required performance in space. Existing computer codes being used to fill this need are known to have deficiencies: e.g. the use of early and incorrect proton damage coefficients at intermediate energies, the inaccurate replacement of non-uniform damage effect by an "equivalent 1-MeV electron" damage which is equivalent only for a specific cell and a specific spectrum, the tedious calculation of coverslide shielding by Monte Carlo techniques, the neglect of changes in the junction parameters, etc. Such deficiencies in these earlier codes make use of the present one advisable, although its results are no more precise than the current state-of-art.

C. New Technology

After a diligent review of the work performed under this contract, it was determined that no new innovation, discovery, improvement or invention was developed.

VI.   GLOSSARY

English Letters

c   velocity of light in a vacuum (cm/sec)

D atomic diffusion coefficient of dopant atoms into silicon (cm^3/sec)

D_n diffusion coefficient of electrons in p-type silicon (cm^3/sec)

D_p diffusion coefficient of holes in n-type silicon (cm^3/sec)

E   electric field in cell due to impurity gradient (volts/cm)

E   energy of a particle in a solar cell (MeV)

E_g energy gap of silicon (1.11 eV)

E_t maximum residual energy of a proton after penetrating a thickness t. (MeV)

E_o energy of a particle incident on a solar cell assembly (MeV)

$G(x)$ rate of production of minority carrier per cm^3 at depth x in silicon (carriers/cm^3 - sec)

$\hbar$ Planck's constant (joule-sec or eV-sec)

h_k increment thickness (cm)

$H(\lambda)$ spectral irradiance outside solar cell assembly, at wavelength λ (watts/cm^2 - micron)

I   Solar cell current through an external load (milliamperes)

I_D Diode current (milliamperes)

I_L photovoltaic current induced in the solar cell (milliamperes)

I_{sc} current from a short circuited solar cell (milliamperes)

I_o diode reverse saturation current of a solar cell (milliamperes)

J   minority carrier current density (milliamperes/cm^3)

K_p, K_e damage coefficient relating proton or electron fluence to degradation in L (dimensionless)

k   Boltzmann's constant (1.38 x 10^{-23} joule/molecule - K^o)

L   base region minority carrier diffusion length (cm)

L_o	base region minority carrier diffusion length before irradiation (cm)
N	concentration of dopant atoms (cm^{-3})
n	parameter from Table 2 for proton range
n	electron concentration in p-type silicon (cm^{-3})
p	hole concentration in n-type silicon (cm^{-3})
P_{max}	maximum power available from a solar cell (milliwatts)
q	unit electric charge (1.602×10^{-19} coulomb)
R	range of a proton in silicon (mg/cm^3)
R	solar cell series resistance (ohms)
R_o	parameter from Table 2 for proton range
T	absolute temperature (degrees Kelvin)
t	process time of dopant diffusion to form n type surface region (sec)
t	coverslide thickness (cm)
U	light intensity incident on the solar cell assembly ($milliwatts/cm^2$)
V	solar cell potential across an external load (millivolts)
V_{oc}	potential across an open circuited solar cell (millivolts)
V_o	solar cell characteristic voltage (millivolts)
x	depth into the solar cell (cm)
x_j	depth of junction below solar cell surface (cm)
z	depth into the solar cell assembly (cm) ($z = t + x$)

Greek Letters

$\alpha(\lambda)$ Absorption coefficient in silicon for light of wavelength λ (cm^{-1})

θ angle between a perpendicular to the solar cell surface and the direction of motion of the particle or photon being considered (degrees)

θ' angle of light ray in silicon, having angle θ in space with respect to normal (degrees)

λ wavelength of light (microns)

μ minority carrier mobility (cm^2/volt - sec)

τ mean lifetime of a minority carrier in the conduction band (sec)

Φ_p, Φ_e proton or electron fluence to which the solar cell assembly has been exposed (cm^{-2})

Ω resistivity of solar cell base region (ohm-cm)

ω 2π times frequency of incident photon (sec^{-1})

REFERENCES

1. Wolf, M.; and Prince, M. B.: New Developments in Silicon
    Photovoltaic Devices and Their Application to Electronics.
    Proceedings of the International Conference in Brussels ·
    2-7 June, 1958.

2. Downing, R. G., et al.: Study of Radiation Effects in
    Lithium Doped Silicon Solar Cells. Final TRW Report on
    JPL Contract 952251, May 1969.

3. Wolf, M.; and Rauschenbach, H.: Series Resistance Effects
    on Solar Cell Measurements. Advanced Energy Conversion,
    vol. 3, 1963, pp. 455-479.

4. Ladany, I.: DC Characteristics of a Junction Diode. Pro-
    ceedings of the IRE. April 1959.

5. Morin, F. J.; and Maita, J. P.: Electrical Properties of Si
    Containing As and B. Phys. Rev., vol. 96, 1954, pp. 28.

6. Reynard, D. L.: Proton and Electron Irradiation of N/P
    Silicon Solar Cells. Report LMSC 3-56-65-4, Lockheed
    Aircraft Corp., April 1965.

7. Bullis, M. W.; and Runyan, W. R.: Influence of Mobility
    Variations on Drift Field Enhancement in Silicon Solar
    Cells. Appendix to NASA Report CR-461. Prepared under
    Contract No. NAS5-3559.

8. Conwell, E. M.: Properties of Silicon and Germanium. Pro-
    ceedings of the IRE., vol. 46, 1958, pp. 1281.

9. Kennerud, K. L.: Electrical Characteristics of Silicon
    Solar Cells at Low Temperatures. IEEE Trans., Aerospace
    and Elec. Systems AES-3, July 1967.

10. Barrett, M. J.; and Stroud, R. H.: A Model for Silicon
    Solar Cell Performance in Space. Final Report (JPL Contract
    952246), Systems Res. Div., Exotech Inc., Feb. 1969.

11. Ritchie, D. W.; and Sandstrom, J. D.: Multikilowatt Solar
    Arrays. In Sixth Photovoltaic Specialists Conf., vol. II,
    March 1967, pp. 180-198.

12. Shockley, W.: Bell System Tech. J. 28,435, 1949.

13. Stroud, R. H.; and Barrett, M. J.: An Analytical Review of
    the ATS-1 Solar Cell Experiment. Final Report (NAS 5-11663),
    Systems Res. Div., Exotech Inc., Nov. 1969.

14. Handy, R. J.: Theoretical Analysis of The Series Resistance of a Solar Cell. Solid State Electronics, vol. 10, March 1967, pp. 765-775.

15. Crowther, D. L., et al.: An Analysis of Nonuniform Proton Irradiation Damage in Silicon Solar Cells. IEEE Trans. on Nuclear Science, NS-13: no. 5, 37-49, Oct. 1966.

16. Johnson, F. S.: Satellite Environment Handbook. Lockheed Aircraft Corp., (Sunnyvale, Calif.), Missiles and Space Division. LMSD-895006 (Tech. Report: Physics), Dec. 1960.

17. Macfarlane, G. C.; and Roberts, V.: Phys. Rev., vol. 97, 1955, pp. 1714; vol. 98, 1955, pp. 1865.

18. Newberger, M.: Silicon Data Sheets DS-137, May 1964 and Silicon Bibliographic Suppl. DS-137 Suppl., July 1968.

19. Janni, F. S.: Calculations of Energy Loss, Path Length, Straggling, Multiple Scattering, and the Probability of Inelastic Collisions for 0.1 to 1000 MeV Protons. Air Force Weapons Laboratory. Tech. Report no. AFWL-TR-65-150, Sept. 1966.

20. Denney, J. M.; and Downing, R. G.: Charged Particle Radiation Damage in Semiconductors, IX: Proton Radiation Damage in Silicon Solar Cells. TRW Space Technology Labs., Redondo Beach, Calif., Final Report on Contract NAS5-1851. TRW 8653-6026-KU-000, Aug. 1963.

21. Barrett, M. J.: Electron Damage Coefficients in P-Type Silicon. IEEE Trans. on Nuc. Sci. no. 6, Dec. 1967.

22. Denney, J. M., et al.: The Energy Dependence of Electron Damage in Silicon. TRW Space Technology Labs., TRW 4141-6004-KU-000, Sept. 1964.

23. Statler, R. L.; and Curtin, D. J.: Low Energy Proton Damage in Partially Shielded and Fully Shielded Silicon Solar Cells. Tech. Memo. CL-24-68, Communications Satellite Corp., Nov. 1968.

24. Iles, P. A.: Study of Lithium Doped Solar Cells. Centralab Semiconductor Division, Globe-Union Inc., Final Report on JPL Contract 952250, June 1969.

APPENDIX: FORTRAN PROGRAM LISTING

The computer program for solar cell performance predictions is listed here. In Fortran IV, it conforms to USA Standards Institute standards. With the program entered in the computer, input variables corresponding to a particular solar cell under consideration are to be entered by changing lines 150 to 270, 290, 940 to 970, and 990. The variables are identified in Table 3, on pp. 28 of this report. Values greater than 200 for M, or greater than 50 for INA are not allowed in the program.

A sample output is presented and discussed in Table 4, on pp. 33 of this report.

```
100 DIMENSION EP(200),XL(200),HX(200),DX(200),C(200)
110 DIMENSION C(200),FS(50),PI(50),CA(50)
120 DIMENSION EOP(10),PHP(10),EOE(10),PHE(10)
130 COMMON/ABSC/DX/INTERV/HX/AMT/C/GABSC/G
140 COMMON/DAMP/EP/DIFF/XL/ENER/ES/FLU/PI/AVG/CA
150 DATA XLO,D,RHO/150.,35.,10./
160 DATA VO,R/43.,.1/
170 DATA T,XJU,CT/14.,.5,6./
180 DATA TEMP,U,THETA/300.,140.,0.0/
190 DATA(EOP(I),I=1,5)/0.0,0.0,0.0,0.0,0.0/
200 DATA(EOP(I),I=6,10)/0.0,0.0,0.0,0.0,0.0/
210 DATA(PHP(I),I=1,5)/0.0,0.0,0.0,0.0,0.0/
220 DATA(PHP(I),I=6,10)/0.0,0.0,0.0,0.0,0.0/
230 DATA(EOE(I),I=1,5)/0.0,0.0,0.0,0.0,0.0/
240 DATA(EOE(I),I=6,10)/0.0,0.0,0.0,0.0,0.0/
250 DATA(PHE(I),I=1,5)/0.0,0.0,0.0,0.0,0.0/
260 DATA(PHE(I),I=6,10)/0.0,0.0,0.0,0.0,0.0/
270 M=200
280 N=M-2
290 INA=50
300 COV=1.0
310 D=D*(TEMP/300.)**(-1.5)
320 XLO=XLO*1E-4*(TEMP/300.)**2.
330 XJU=XJU*1.E-4
340 CT=CT*2.54E-3
350 T=T*2.54E-3
360 IF(CT.NE.0.0)GO TO 5
370 COV=0.0
380 CT=XJU
390 5 DO 10 I=1,M
400 10 XL(I)=XLO
410 CALL ABSCIS (M,T,XJU)
420 CALL LIGHT (M,TEMP,U,THETA)
430 DO 30 IN=1,10
440 EO=EOP(IN)
450 PHI=PHP(IN)
460 IF(EO.LE..9E-4)GO TO 30
470 IF(EO.GE.200.)GO TO 30
480 IF(PHI.EQ.0.0)GO TO 30
490 CALL COVER (EO,CT,PHI,XJU,COV,INA)
500 DO 20 MM=1,INA
510 IF(ES(MM).LE..9E-4)GO TO 30
520 CALL PROTON (XJU,M,MM,COV)
530 CALL DAMAGE (M,MM,RHO)
540 20 CONTINUE
550 30 CONTINUE
560 DO 60 IN=1,10
570 EO=EOE(IN)
580 PHI=PHE(IN)
590 IF(EO.LE..25)GO TO 60
600 IF(EO.GE.40.)GO TO 60
610 IF(PHI.EQ.0.0)GO TO 60
620 CALL ELECT (EO,PHI,M,COV,XJU,CT,RHO)
630 60 CONTINUE
640 CON=XL(2)
650 CALL ROOT(N,M,D,XJU)
660 CALL CURVE (D,TEMP,U,VO,R,CON,XLO,XJU,THETA)
670 STOP
680 END
```

43.

```
690 *
700 *
710 *
720 SUBRØUTINE ABSCIS (M,T,XJU)
730 DIMENSIØN DX(200),HX(200)
740 CØMMØN /ABSC/DX/INTERV/HX
750 FLØ=FLØAT(M-20)
760 DELTA=(T-XJU)/(FLØ*(FLØ-1.)/2.+20.)
770 KK=M-1
780 DX(1)=XJU
790 DØ 10 I=1,20
800 HX(I)=DELTA
810 10 DX(I+1)=DX(I)+HX(I)
820 DØ 5 I=21,KK
830 HX(I)=FLØAT(I-20)*DELTA
840 5 DX(I+1)=DX(I)+HX(I)
850 DX(M)=T
860 RETURN
870 END
880 *
890 *
900 *
```

44.

```
 910 SUBROUTINE LIGHT (M,TEMP,U,THETA)
 920 DIMENSION A(15),H(15),S(15),R(15),DX(200),G(200)
 930 COMMON/ABSC/DX/GABSC/C
 940 DATA(A(I),I=1,15)/75000.,25800.,11800.,7000.,4650.,3330.,2420.,
 950+ 1690.,1120.,795.,380.,180.,73.,20.8,4.4/
 960 DATA(H(I),I=1,15)/.154,.22,.198,.195,.181,.162,.144,
 970+ .127,.1127,.1003,.0895,.0803,.0725,.0665,.0606/
 980 IF(THETA.EQ.0.0)GO TO 20
 990 CIN=3.8
1000 ARG=THETA*.017453
1010 AC=COS(ARG)
1020 AS=SIN(ARG)
1030 AP=ATAN(AS/(CIN*(1.-(AS/CIN)**2.)))
1040 AS=COS(AP)
1050 GO TO 30
1060 20 AC=1.
1070 AS=1.
1080 30 DO 10 I=1,15
1090 H(I)=H(I)*U*AC/140.
1100 10 A(I)=A(I)*(3.323*EXP(-702.6/TEMP)+1.)/1.319
1110 P=6.625E-34
1120 V=2.998E8
1130 DEN=P*V
1140 W=0.4
1150 I=1
1160 COE=0.05/3.
1170 S(I)=COE*W*H(I)*A(I)
1180 COE=COE*2.
1190 35 W=W+0.05
1200 I=I+1
1210 S(I)=COE*(1.+FLOAT(MOD(I+1,2)))*W*H(I)*A(I)
1220 IF(I.LT.14)GO TO 35
1230 W=W+0.05
1240 S(15)=(COE/2.)*W*H(15)*A(15)
1250 DO 45 J=1,M
1260 GG=0.0
1270 DO 54 I=1,15
1280 R(I)=S(I)*1.E-6*EXP(-A(I)*DX(J)/AS)
1290 54 GG=GG+R(I)
1300 45 G(J)=GG/DEN
1310 RETURN
1320 END
1330 *
1340 *
1350 *
```

45.

```fortran
1360 SUBRØUTINE CØVER (EØ,CT,PHI,XJU,CØV,INA)
1370 DIMENSIØN E(5),R1(4),ET1(4),ES(50),PI(50),CA(50)
1380 DIMENSIØN ET(4),RO(4),R1C(4),ROC(4)
1390 CØMMØN/ENER/ES/FLU/PI/ANG/CA
1400 DATA(E(I),I=1,5)/0.0,.3,.8,2.,200./
1410 DATA(ROC(I),I=1,4)/2.81,3.945,4.11,3.42/
1420 DATA(ET(I),I=1,4)/.995,1.277,1.46,1.726/
1430 DATA(R1C(I),I=1,4)/2.07,3.04,3.18,2.85/
1440 DATA(ET1(I),I=1,4)/1.057,1.375,1.576,1.73/
1450 IF(CØV.NE.0.0)GØ TØ 5
1460 DØ 6 I=1,4
1470 R1(I)=ROC(I)/2.33E3
1480 6 ET1(I)=ET(I)
1490 GØ TØ 7
1500 5 DØ 47 I=1,4
1510 47 R1(I)=R1C(I)/2.2E3
1520 7 DØ 3 I=1,4
1530 IF(E(I+1).GT.EØ)GØ TØ 4
1540 3 CØNTINUE
1550 GØ TØ 16
1560 4 RØ=R1(I)*(EØ**ET1(I))
1570 IF(RØ.LE.CT)GØ TØ 16
1580 EC=(EØ**ET1(I)-CT/R1(I))**(1./ET1(I))
1590 IF(EC.LE..9E-4)GØ TØ 16
1600 FAC=EØ**ET1(I)
1610 AR=CT/(R1(I)*(FAC-.9E-4**ET1(I)))
1620 TAN=SQRT(1.-AR**2)/AR
1630 AN=ATAN(TAN)
1640 STEP=AN/FLØAT(INA)
1650 XI1=1./(FAC-EC**ET1(I))
1660 AR=0.0
1670 DØ 18 K=1,INA
1680 CA(K)=CØS(AR+.5*STEP)
1690 ES(K)=(FAC-CT/(R1(I)*CA(K)))**(1./ET1(I))
1700 XI2=XI1
1710 XI1=FAC-CT/(R1(I)*CØS(AR+STEP))
1720 XI1=1./(FAC-XI1)
1730 PI(K)=PHI*CT*(XI2-XI1)/R1(I)
1740 18 AR=AR+STEP
1750 XI1=.9E-4**ET1(I)
1760 XI1=1./(FAC-XI1)
1770 PI(INA)=PHI*CT*(XI2-XI1)/R1(I)
1780 GØ TØ 19
1790 16 ES(1)=0.0
1800 19 RETURN
1810 END
1820 *
1830 *
1840 *
```

Note: Instruction 1510 applies to solar cells with Corning 7940 coverslides. For sapphire, with a density of 3.98 gm/cm^3, this becomes

```fortran
1510 47 R1(I)=R1C(I)/3.98E3
```

```
1850 SUBRØUTINE PRØTØN (XJU,M,MM,CØV)
1860 DIMENSIØN HX(200),EP(200),ES(50),CA(50)
1870 DIMENSIØN E(5),RØ(4),ET(4),ROC(4)
1880 CØMMØN/INTERV/HX/DAMP/EP/ENER/ES/ANC/CA
1890 DATA(E(I),I=1,5)/0.0,.3,.8,2.,200./
1900 DATA(ROC(I),I=1,4)/2.81,3.945,4.11,3.42/
1910 DATA(ET(I),I=1,4)/.995,1.277,1.46,1.726/
1920 EP(1)=ES(MM)
1930 DØ 47 I=1,4
1940 47 RØ(I)=ROC(I)/2.33E3
1950 K=1
1960 DØ 21 I=1,4
1970 IF(E(I+1).GT.EP(1))CØ TØ 22
1980 21 CØNTINUE
1990 22 RØ=CA(MM)*RØ(I)*(EP(1)**ET(I)).
2000 IF(CØV.EQ.0.0)GØ TØ 50
2010 IF(RØ.LT.XJU)CØ TØ 16
2020 EP(1)=(EP(1)**ET(I)-XJU/(RØ(I)*CA(MM)))**(1./ET(I))
2030 50 IF(EP(1).LE..9E-4)GØ TØ 16
2040 DØ 6 K=2,M
2050 RØ=CA(MM)*RØ(I)*(EP(K-1)**ET(I))
2060 IF(HX(K-1).GT.RØ)CØ TØ 16
2070 EP(K)=(EP(K-1)**ET(I)-HX(K-1)/(RØ(I)*CA(MM)))**(1./ET(I))
2080 IF(EP(K).LE..9E-4)GØ TØ 16
2090 IF(EP(K).GT.E(I))CØ TØ 6
2100 I=I-1
2110 6 CØNTINUE
2120 CØ TØ 14
2130 16 EP(K)=0.0
2140 14 RETURN
2150 END
2160 *
2170 *
2180 *
2190 SUBRØUTINE DAMAGE (M,MM,RHØ)
2200 DIMENSIØN EP(200),XL(200),PI(50)
2210 CØMMØN/DIFF/XL/DAMP/EP/FLU/PI
2220 ØME=RHØ**(-.75)
2230 DØ 19 I=1,M
2240 IF(EP(I).LT.3.)GØ TØ 20
2250 19 EP(I)=1.2E-5*ØME*(EP(I)**(-.9))
2260 GØ TØ 14
2270 20 DEA=EXP(-1.04)
2280 ØME=ØME*1.92E-5
2290 DØ 21 J=I,M
2300 IF(EP(J).LT..1.)GØ TØ 22
2310 21 EP(J)=ØME*DEA*((EP(J)/.962)**(-.85))
2320 GØ TØ 14
2330 22 DØ 23 I=J,M
2340 IF(EP(I).LE..9E-4)GØ TØ 14
2350 23 EP(I)=ØME*EXP(-1.08*EP(I))
2360 14 DØ 5 I=1,M
2370 IF(EP(I).EQ.0.0)GØ TØ 24
2380 A=XL(I)*XL(I)
2390 5 XL(I)=SQRT(A/(A*PI(MM)*EP(I)+1.0))
2400 24 RETURN
2410 END
```

```
2420 *
2430 *
2440 *
2450 SUBRØUTINE ELECT (EØ,PHI,M,CØV,XJU,CT,RHØ)
2460 DIMENSIØN EP(200),HX(200),XL(200)
2470 CØMMØN/DAMP/EP/INTERV/HX/DIFF/XL
2480 ØME=((10./RHØ)**.5)*1E-10
2490 EXN=-10./(EØ**1.5)
2500 IF(EØ.LE.1.)GØ TØ 10
2510 DC=ØME*(1.2*ALØG(2.17*EØ))**2.
2520 GØ TØ 20
2530 10 DC=ØME*(.67*ALØG(4.*EØ))**2.
2540 20 TH=CØV*CT*2.2+XJU*2.33
2550 EP(1)=DC*EXP(EXN*TH)
2560 A=XL(1)**2.
2570 XL(1)=SQRT(A/(A*PHI*EP(1)+1.))
2580 DØ 40 I=2,M
2590 TH=TH+HX(I-1)*2.33
2600 EP(I)=DC*EXP(EXN*TH)
2610 A=XL(I)**2.
2620 40 XL(I)=SQRT(A/(A*PHI*EP(I)+1.))
2630 RETURN
2640 END
2650 *
2660 *
2670. *
```

Note: Instruction 2540 applies to solar cells with Corning 7940 coverslides. For sapphire, with a density of 3.98 gm/cm^3, this becomes

2540 20 ....

```
2680 SUBROUTINE ROOT (N,M,D,XJU)
2690 DIMENSION HX(200),DX(200),XL(200)
2700 DIMENSION C(200),G(200),EP(200)
2710 COMMON/ABSC/DX/INTERV/HX/DIFF/XL
2720 COMMON/GABSC/G/DAMP/EP/AMT/C
2730 DO 119 K=1,N
2740 HSUM=HX(K)+HX(K+1)
2750 DX(K)=1./(XL(K+1)**2.)+2./(HX(K+1)*HX(K))
2760 XL(K)=2./(HX(K)*HSUM)
2770 EP(K)=2./(HX(K+1)*HSUM)
2780 DX(K)=DX(K)/EP(K)
2790 XL(K)=XL(K)/EP(K)
2800 EP(K)=C(K+1)/(D*EP(K))
2810 119 CONTINUE
2820 C(1)=0.0
2830 C(2)=1.0E8
2840 C2H=0.0
2850 C2L=0.0
2860 K=0
2870 5 CONTINUE
2880 CALL TRAP (N,K)
2890 IF(C(K+2))10,20,30
2900 20 IF(M-K)10,40,10
2910 10 C2L=C(2)
2920 C(2)=C(2)*10.
2930 IF(C2L*C2H)50,5,50
2940 30 C2H=C(2)
2950 C(2)=C(2)/10.
2960 IF(C2L*C2H)50,5,50
2970 50 C(2)=(C2L+C2H)/2.
2980 TEST=(C2H-C2L)/C2H
2990 IF(TEST.LT.1.0E-6)GO TO 40
3000 CALL TRAP (N,K)
3010 IF(C(K+2))60,70,80
3020 70 IF(M-K)60,40,60
3030 60 C2L=C(2)
3040 GO TO 50
3050 80 C2H=C(2)
3060 GO TO 50
3070 40 RETURN
3080 END
3090 *
3100 *
3110 *
3120 SUBROUTINE TRAP (N,K)
3130 DIMENSION C(200),DX(200),EP(200),XL(200)
3140 COMMON/ABSC/DX/DIFF/XL/DAMP/EP/AMT/C
3150 DO 99 K=1,N
3160 C(K+2)=C(K+1)*DX(K)-C(K)*XL(K)-EP(K)
3170 IF(C(K+2).GT.1.E30)GO TO 50
3180 IF(C(K+2).LT.0.0)GO TO 50
3190 99 CONTINUE
3200 50 RETURN
3210 END
```

```
3220 *
3230 *
3240 *
3250 SUBROUTINE CURVE (D,TEMP,U,VO,R,CON,XLO,XJU,THETA)
3260 DIMENSION C(200),HX(200)
3270 COMMON/AMT/C/INTERV/HX
3280 10 FORMAT(3HIL=,F6.2,3H MA,10X,2HU=,F6.1,9H MW/CM**2)
3290 20 FORMAT(3HVO=,F6.2,3H MV,10X,5HTEMP=,F5.0,7H DEG. K)
3300 30 FORMAT(2HR=,F6.3,4H OHM,10X,6HTHETA=,F6.2,5H DEG.)
3310 50 FORMAT(3HIO=,E10.3,3H MA,//)
3320 70 FORMAT(8X,5HI(MA),4X,5HV(MV),4X,5HP(MW),/)
3330 80 FORMAT(7X,F6.2,3X,F6.1,3X,F6.2)
3340 Q1=1.602E-19
3350 UN=U*COS(THETA*.017453)
3360 CU=Q1*D*C(2)*1.E3/HX(1)
3370 CS=.42543*ALOG(XJU*1E4)+1.0057-1.0079*EXP(-53530.*CON)
3380 CS=CS*(TEMP+400.)*UN*1E-4
3390 CU=CU+CS
3400 CIO=(XLO/CON)*(1.572*ALOG(UN)-3.36)*1E5
3410 CIO=CIO*EXP(-6492.75/TEMP)
3420 WRITE(9,10)CU,U
3430 WRITE(9,20)VO,TEMP
3440 WRITE(9,30)R,THETA
3450 WRITE(9,50)CIO
3460 WRITE(9,70)
3470 STEP=CU/10.
3480 DO 40 I=1,10
3490 XI=STEP*FLOAT(I-1)
3500 V=VO*ALOG((CU+CIO-XI)/CIO)-XI*R
3510 P=XI*V*1E-3
3520 40 WRITE(9,80)XI,V,P
3530 STEP=(CU-XI)/10.
3540 DO 60 I=1,10
3550 XI=XI+STEP
3560 V=VO*ALOG((CU+CIO-XI)/CIO)-XI*R
3570 P=XI*V*1E-3
3580 60 WRITE(9,80)XI,V,P
3590 RETURN
3600 END
```

50.